NeuroImage: Clinical 17 (2018) 347–353

Contents lists available at ScienceDirect

NeuroImage: Clinical

journal homepage: www.elsevier.com/locate/ynicl

Imaging of glia activation in people with primary lateral sclerosis

Sabrina Paganoni[a,b], Mohamad J. Alshikho[a,c], Nicole R. Zürcher[c], Paul Cernasov[a], Suma Babu[a], Marco L. Loggia[c], James Chan[d], Daniel B. Chonde[c], David Izquierdo Garcia[c], Ciprian Catana[c], Caterina Mainero[c], Bruce R. Rosen[c], Merit E. Cudkowicz[a], Jacob M. Hooker[c], Nazem Atassi[a,*]

[a] Harvard Medical School, Department of Neurology, Neurological Clinical Research Institute (NCRI), Massachusetts General Hospital, Boston, MA, USA
[b] Harvard Medical School, Department of Physical Medicine and Rehabilitation, Spaulding Rehabilitation Hospital, Charlestown, MA, USA
[c] A. A. Martinos Center for Biomedical Imaging, Department of Radiology, Massachusetts General Hospital, Harvard Medical School, Charlestown, MA, USA
[d] Biostatistics Center, Massachusetts General Hospital, Boston, MA, USA

ARTICLE INFO

Keywords:
Diffusion
PET
TSPO
Primary lateral sclerosis
Amyotrophic lateral sclerosis
[^{11}C]-PBR28

ABSTRACT

Background: Glia activation is thought to contribute to neuronal damage in several neurodegenerative diseases based on preclinical and human *post-mortem* studies, but its role in primary lateral sclerosis (PLS) is unknown.
Objectives: To localize and measure glia activation in people with PLS compared to healthy controls (HC).
Methods: Ten participants with PLS and ten age-matched HCs underwent simultaneous magnetic resonance (MR) and proton emission tomography (PET). The radiotracer [^{11}C]-PBR28 was used to obtain PET-based measures of 18 kDa translocator protein (TSPO) expression, a marker of activated glial cells. MR techniques included a structural sequence to measure cortical thickness and diffusion tensor imaging (DTI) to assess white matter integrity.
Results: PET data showed increased [^{11}C]-PBR28 uptake in anatomically-relevant motor regions which co-localized with areas of regional gray matter atrophy and decreased subcortical fractional anisotropy.
Conclusions: This study supports a link between glia activation and neuronal degeneration in PLS, and suggests that these disease mechanisms can be measured *in vivo* in PLS. Future studies are needed to determine the longitudinal changes of these imaging measures and to clarify if MR-PET with [^{11}C]-PBR28 can be used as a biomarker for drug development in the context of clinical trials for PLS.

1. Introduction

Glia activation has been implicated in the pathogenesis of several neurodegenerative diseases based on both pre-clinical and human *post-mortem* studies. For instance, glia activation has been detected in animal models and human CNS autopsy tissue in Alzheimer's disease (AD) (Yin et al., 2017; Griciuc et al., 2013; Kreisl et al., 2016), amyotrophic lateral sclerosis (ALS) (Alexianu et al., 2001; Brettschneider et al., 2012), multiple sclerosis (MS) (Brettschneider et al., 2012; Franciosi et al., 2012) and Huntington's disease (HD) (Franciosi et al., 2012; Sapp et al., 2001). Work in mouse models of ALS suggest that glia activation contributes to disease progression and neurotoxicity (Boillee et al., 2006; Beers et al., 2006; Zhao et al., 2004). ALS is a form of motor neuron disease (MND) where both the upper and lower motor neurons are progressively lost whereas primary lateral sclerosis (PLS) is an MND that predominantly affects the neurons that arise from the motor cortex (Upper Motor Neurons, UMNs) (Statland et al., 2015). The role of glia activation in PLS is unknown.

Glia activation can be tracked *in vivo* by using PET radiotracers such as [^{11}C]-PBR28 that bind to the 18 kDa translocator protein (TSPO). [^{11}C]-PBR28 uptake is low in healthy brain tissue, but is increased in the setting of microglia activation and reactive astrocytosis (Lavisse et al., 2015). Further, PET can be combined with magnetic resonance (MR) techniques to assess white matter integrity (diffusion tensor imaging or DTI) and neuronal loss (morphometric analyses). This type of multimodal neuroimaging can deliver a snapshot of complex disease mechanisms *in vivo* and may represent a novel tool to track disease severity, progression, and response to candidate treatments. Indeed, there is growing interest in multimodal neuroimaging across neurologic disease as shown by recent proof-of-concept studies suggesting that MR-

* Corresponding author at: Neurological Clinical Research Institute (NCRI), Massachusetts General Hospital, 165 Cambridge Street, Suite 656, Boston, 02114, MA, USA.
E-mail addresses: spaganoni@mgh.harvard.edu (S. Paganoni), malshikho@mgh.harvard.edu (M.J. Alshikho), zurcher@nmr.mgh.harvard.edu (N.R. Zürcher), paul.cernasov@gmail.com (P. Cernasov), sbabu@mgh.harvard.edu (S. Babu), marco@nmr.mgh.harvard.edu (M.L. Loggia), jchan12@mgh.harvard.edu (J. Chan), chonde@mit.edu (D.B. Chonde), davidizq@nmr.mgh.harvard.edu (D.I. Garcia), ccatana@nmr.mgh.harvard.edu (C. Catana), caterina@nmr.mgh.harvard.edu (C. Mainero), bruce@nmr.mgh.harvard.edu (B.R. Rosen), mcudkowicz@mgh.harvard.edu (M.E. Cudkowicz), hooker@nmr.mgh.harvard.edu (J.M. Hooker), natassi@mgh.harvard.edu (N. Atassi).

http://dx.doi.org/10.1016/j.nicl.2017.10.024
Received 18 August 2017; Received in revised form 21 October 2017; Accepted 24 October 2017
Available online 25 October 2017

PET can be used to identify glia activation and its relationship to neuronal loss and structural abnormalities in AD,(Kreisl et al., 2016; Kreisl et al., 2013), ALS (Zurcher et al., 2015; Alshikho et al., 2016; Turner et al., 2004; Corcia et al., 2012), HD (Politis et al., 2011; Tai et al., 2007), and in populations with a history of concussion or moderate-to-severe traumatic brain injury (Coughlin et al., 2015; Coughlin et al., 2017; Ramlackhansingh et al., 2011).

While the course of PLS is slower and the prognosis is more favorable than ALS, it still leads to progressive disability including difficulty walking, difficulty performing activities of daily living, dysarthria, and dysphagia. There are no available treatments that slow down PLS disease progression. Further, there are no animal models of PLS, no available biomarkers, and patients with PLS are usually excluded from ALS clinical trials because it is unclear if they share the same pathophysiology. Elucidating *in vivo* disease mechanisms is clearly an unmet need for this orphan disease. Here we employed MR-PET to test the hypothesis that people with PLS have increased glia activation in the motor regions, and that glia activation co-localizes and correlates with cortical thinning (suggestive of neuronal loss) and white matter dysfunction. The hypothesis is anchored on autopsy reports from PLS patients showing glia proliferation surrounding areas of motor neuron loss in the motor cortices (Beal and Richardson, 1981; Hudson et al., 1993; Pringle et al., 1992).

2. Materials and methods

2.1. Study participants

Ten individuals with PLS (7 men, 3 women; mean age [SD] in years, 62 [8.5]) and ten age-matched healthy controls (5 men, 5 women; mean age [SD] in years, 54 [11.3]) were included in the study. To meet inclusion criteria, PLS participants had to meet Pringle's criteria for the diagnosis of PLS (Pringle et al., 1992). Diagnosis was confirmed at enrollment by a physician with sub-specialty training in Neuromuscular Medicine and expertise in PLS. Since the Ala147Thr polymorphism in the TSPO gene imparts a trimodal pattern of binding affinity to second generation TSPO ligands such as [^{11}C]-PBR28 (Owen et al., 2012), the participants in both groups were genotyped for this polymorphism at screening in order to exclude low affinity binders (Thr/Thr), and to match the proportion of high- (Ala/Ala) and mixed-affinity binders (Ala/Thr) across groups (4 and 6, respectively in both groups). The study was approved by the Partners Human Research Committee and the Radioactive Drug Research Committee. All participants provided written informed consent.

2.2. Clinical assessments

Clinical assessment included the revised ALS functional rating scale (ALSFRS-R) (Cedarbaum et al., 1999) and the upper motor neuron burden scale (UMNB) (Zurcher et al., 2015). The ALSFRS-R is a 12-question ordinal rating scale (ratings 0–4) that is widely used to measure functional status in patients with motor neuron disease. The scale ranges from 48 (normal level of functioning) to zero, with lower scores indicating increased disability. The scale evaluates function in four domains: gross and fine motor function, bulbar function, and breathing. Vital capacity was assessed using a portable spirometer and expressed as percent of predicted for age, gender and height. Demographic information and clinical assessments are summarized in Table 1.

2.3. MR-PET imaging

All participants had simultaneous MR-PET imaging using the radiotracer [^{11}C]-PBR28. [^{11}C]-PBR28 was produced in-house as previously described (Imaizumi et al., 2007). The radiotracer was administered as a slow intravenous bolus. Mean [SD] administered dose of [^{11}C]-PBR28 was 495 MBq [66.47] for PLS participants and 450 MBq [53] for HC, *not significant*.

Table 1
Demographic and clinical characteristics of study participants.

	PLS	HC
Number of participants	10	10
Male/female	7/3	5/5
Age range (years)	44.3–70.3	31.7–65.3
Age (years, mean ± SD)	61.8 y ± 8.54	54.03 y ± 11.3
TSPO genotype		
Ala/Ala (high affinity binding)	4/10	4/10
Ala/Thr (mixed affinity binding)	6/10	6/10
Disease duration (months, mean ± SD)	140.1 ± 56.3	
Range of disease duration (months)	62.3–216.6	
Limb onset	8/10	
ALSFRS-R (mean ± SD)	31.9 ± 7.06	
UMNB (mean ± SD)	31.7 ± 3.13	
Vital capacity (mean ± SD)	83.1% ± 16.06	

Abbreviations: Ala = alanine; ALSFRS-R = amyotrophic lateral sclerosis functional rating scale revised; HC = healthy control; PLS = primary lateral sclerosis; SD = standard deviation; Thr = threonine; TSPO = translocator protein; UMNB = upper motor neuron burden scale. Vital capacity is expressed as percent of predicted for age, sex and height.

MR-PET images were acquired simultaneously from all participants using a Siemens 3T Magnetom Tim Trio scanner (Siemens Erlangen, Germany) with PET insert. This scanner is equipped with an 8-channel head coil. PET data was acquired for 90 min after radio-tracer injection. MR data included T1-weighted 3D multi-echo magnetization prepared rapid acquisition gradient echo (MEMPRAGE) and diffusion weighted imaging (DWI). The diffusion data was obtained at $b = 3000$ s/mm^2 using a single-shot, spin-echo and echo-planar imaging (EPI) sequence with twice refocused spin echo diffusion preparation (Q-ball imaging). Each set of diffusion data included sixty diffusion images and eight non-collinear directions. Acquisition parameters for MR are available online (eTable 1 in the Supplement).

2.4. MR-PET data analyses

FreeSurfer version 6.0 tools were used for T1 image pre-processing including reconstruction, parcellation of cortical surfaces, and segmentation of sub-cortical regions. FreeSurfer was used to perform surface-based analyses (SBA). The FMRIB software library (FSL, v.5.0.9; Oxford, UK) was used to create diffusion maps for fractional anisotropy (FA) and diffusivities (mean MD, axial AD, and radial RD). Preprocessing steps of diffusion data including motion evaluation were conducted as previously reported (Alshikho et al., 2016). [^{11}C]-PBR28 PET data was reconstructed as previously described (Zurcher et al., 2015). Standardized uptake value (SUV) normalized to whole brain mean (SUVR) from 60 to 90 min post time of injection were used to assess TSPO expression ($SUVR_{60–90\ min}$). Finally, the individual $SUVR_{60–90\ min}$ images were registered to the standard MNI template (Montreal Neurological Institute MNI152) to conduct between-group analyses.

2.5. Statistical analyses

2.5.1. Voxel-wise SUVR analysis

$SUVR_{60–90\ min}$ images in MNI152 standard space were fed into a voxel-wise between-groups analysis. Non-parametric permutation inference was performed using 5000 permutations and threshold-free cluster enhancement (TFCE). The resultant statistical maps were family-wise error (FWE) adjusted ($p_{FWE} < 0.05$) to correct for multiple comparisons. General linear model (GLM) was used in the voxel-wise analyses and covariates were added to adjust for the effect of age, sex and [^{11}C]-PBR28 binding affinity.

2.5.2. Surface-based analyses (SBAs)

SBAs were employed to investigate the difference between groups in cortical thickness and [^{11}C]-PBR28 uptake. The analyses were conducted in the pial surface (which follows the border between gray matter and cerebrospinal fluid), as well as in sub-cortical white matter surface (which follows the border between white and gray matter). For SBA analysis of cortical thickness, age and sex were entered as covariates while for SBA of PET data, age, sex and [^{11}C]-PBR28 binding affinity were entered as covariates.

Cortical thickness processed in FreeSurfer version 6.0 and smoothed at full width at half maximum (FWHM) = 6 mm was then fed into SBA. The resultant statistical maps were cluster-wise corrected for multiple comparisons using Monte Carlo simulation.

SBA of SUVR was performed using PET Surfer, a set of tools within FreeSurfer version 6.0 that include correction of partial volume effects. The resultant SUVR images resampled onto brain surface were then smoothed at (FWHM = 6 mm) and fed into a GLM analysis to study on surface the difference in [^{11}C]-PBR28 uptake between groups. A projection factor (projfrac) was used in SBA to project the SUVR maps onto the brain surface. The default value for projfrac is between (0 and 1). Zero represents the border line between white and pial. The negative values of the projfrac (*e.g.* projfrac = −2) means (2 ∗ thickness) away from the white surface into the white matter. To define which layer of the brain has the maximum [^{11}C]-PBR28 uptake difference between groups, multiple values of projfrac (+0.5, 0, −0.5, −1, −1.5, −2) were tested in a separate SBA analysis. The resultant SUVR images, which were resampled onto the brain surface, were then organized by group, concatenated together, smoothed at (FWHM = 6 mm), and fed into a GLM analysis to study the difference in [^{11}C]-PBR28 uptake between groups on the surface. Monte Carlo simulation was used to correct data for multiple companions.

2.5.3. Tract-based spatial statistics (TBSS) analysis

We performed statistical analysis to study differences in FA values between PLS and controls. In this analysis, FA maps were fed into non-parametric permutation inference. Data were permuted (n = 5000), threshold free cluster enhancement (TFCE) method was applied, and the p values were FWE adjusted at p = 0.05 to correct for multiple comparisons. The anatomical locations were determined by using the JHU White-Matter Tractography and JHU ICBM-DTI-81 White-Matter Labels atlases (Wakana et al., 2007; Hua et al., 2008). GLM was used in TBSS to adjust FA values for the effect of age.

2.5.4. Region of Interest (ROI) analysis

The *a priori* ROI was defined to encompass the precentral and paracentral gyri bilaterally (motor region) based on FreeSurfer cortical reconstruction of the standard template MNI152. MR-PET measures ([^{11}C]-PBR28 $SUVR_{60–90\ min}$, FA, MD, AD, and RD) were then computed within this ROI and corrected by age. Statistical analyses were performed using JMP pro 13.0.0 (SAS Institute Inc., Cary, NC, 1989–2014). Between-groups differences were tested using non-parametric Wilcoxon test. Spearman correlation coefficient was used to investigate the relationship between [^{11}C]-PBR28 uptake and FA within the ROI and clinical measures (ALSFRS-R, UMNB, vital capacity, and disease duration). Effect size (Cohen d and 95% confidence interval (CI)) was calculated based on differences between groups.

3. Results

3.1. Mean group [^{11}C]-PBR28 uptake and voxel-wise analysis for between-group differences

Whole brain voxel-wise analysis showed increased [^{11}C]-PBR28 uptake in the motor regions in individuals with PLS compared to healthy controls in both hemispheres (Fig. 1 A,B,C,E). There were no regions for which PLS showed less [^{11}C]-PBR28 uptake than healthy controls. There were no significant right-to-left differences in clinical presentation as measured by UMN Burden scores in this cohort.

3.2. Tract-based spatial statistics (TBSS) analysis

TBSS analysis revealed decreased FA in PLS compared to controls, even after adjusting for age (Fig. 1D), in the left and right corticospinal tracts, left and right superior longitudinal fasciculus and in the body of the corpus callosum (all $p_{FWE} < 0.05$).

3.3. Surface-based (SBA) analyses

SBA of cortical thickness revealed cortical thinning in PLS compared to HC in the precentral gyri ($p < 0.01$) (Fig. 2A) which colocalized with regions of increased [^{11}C]-PBR28 uptake in the subcortical white matter of the motor regions (Fig. 2B).

3.4. Region of interest (ROI) analyses

The anatomical boundaries of the ROI used in this study are shown in Fig. 3A and include the precentral and paracentral gyri bilaterally. In this region, mean [^{11}C]-PBR28 uptake and radial diffusivity were significantly higher in PLS than HC ($p < 0.05$) while FA values were significantly lower ($p < 0.05$) (Fig. 3B).

Table 2 includes differences in RD, AD and MD between groups.

[^{11}C]-PBR28 uptake in the brains of people with PLS showed no significant correlations with FA [r = +0.17; p = 0.62], cortical thickness [r = −0.38; p = 0.28], ALSFRS-R scores [r = +0.33; p = 0.35], UMNB scores [r = +0.26; p = 0.46], vital capacity [r = +0.26; p = 0.47], or disease duration [r = −0.52; p = 0.12]). FA significantly correlated with ALSFRS-R total score [r = +0.85; p = 0.002] but not with UMNB [r = −0.04; p = 0.89], vital capacity [r = +0.37; p = 0.29], or disease duration [r = −0.32; p = 0.36]).

4. Discussion

Our study demonstrates increased *in vivo* glia activation in the motor regions in people with PLS, as measured by [^{11}C]-PBR28 PET imaging. [^{11}C]-PBR28 binds to TSPO, whose expression is dramatically upregulated in activated glial cells including microglia and astrocytes (Lavisse et al., 2015; Rupprecht et al., 2010). This report represents the first step in the development of [^{11}C]-PBR28 PET as an *in vivo* PLS biomarker, an approach that is aligned with efforts that are unfolding in other neurologic diseases (Coughlin et al., 2017; Brier et al., 2016; Passamonti et al., 2017; Gomperts et al., 2016; Herranz et al., 2016). The translational potential of these findings is that [^{11}C]-PBR28 PET signal could be further developed as a biomarker to support proof-of-mechanism trials of compounds that target glia activation in PLS.

Our findings are consistent with autopsy reports from PLS patients showing glia proliferation surrounding areas of motor neuron loss in the motor cortices (Beal and Richardson, 1981; Hudson et al., 1993; Pringle et al., 1992). Increased glia activation overlapped with areas of cortical thinning and white matter abnormalities. Thus, MR-PET can be used to simultaneously capture *in vivo* molecular and structural changes that underlie PLS disease biology. Cortical thinning and white matter abnormalities have been reported previously in PLS (Iwata et al., 2011; Kwan et al., 2012; Canu et al., 2013; Butman and Floeter, 2007; Tartaglia et al., 2009). Here, we confirm these findings and show co-localization with a molecular marker of glia activation.

There is growing evidence that glia activation and phenotypic changes occur during disease progression of motor neuron disease and that microglia exert both neuroprotective and neurotoxic effects at various stages of the disease (Boillee et al., 2006; Beers et al., 2006; Zhao et al., 2004; Appel et al., 2011; Liao et al., 2012). Other glial cells, such as reactive astrocytes, are also proliferated in motor neuron disease (Vargas and Johnson, 2010). While these glia changes denote the

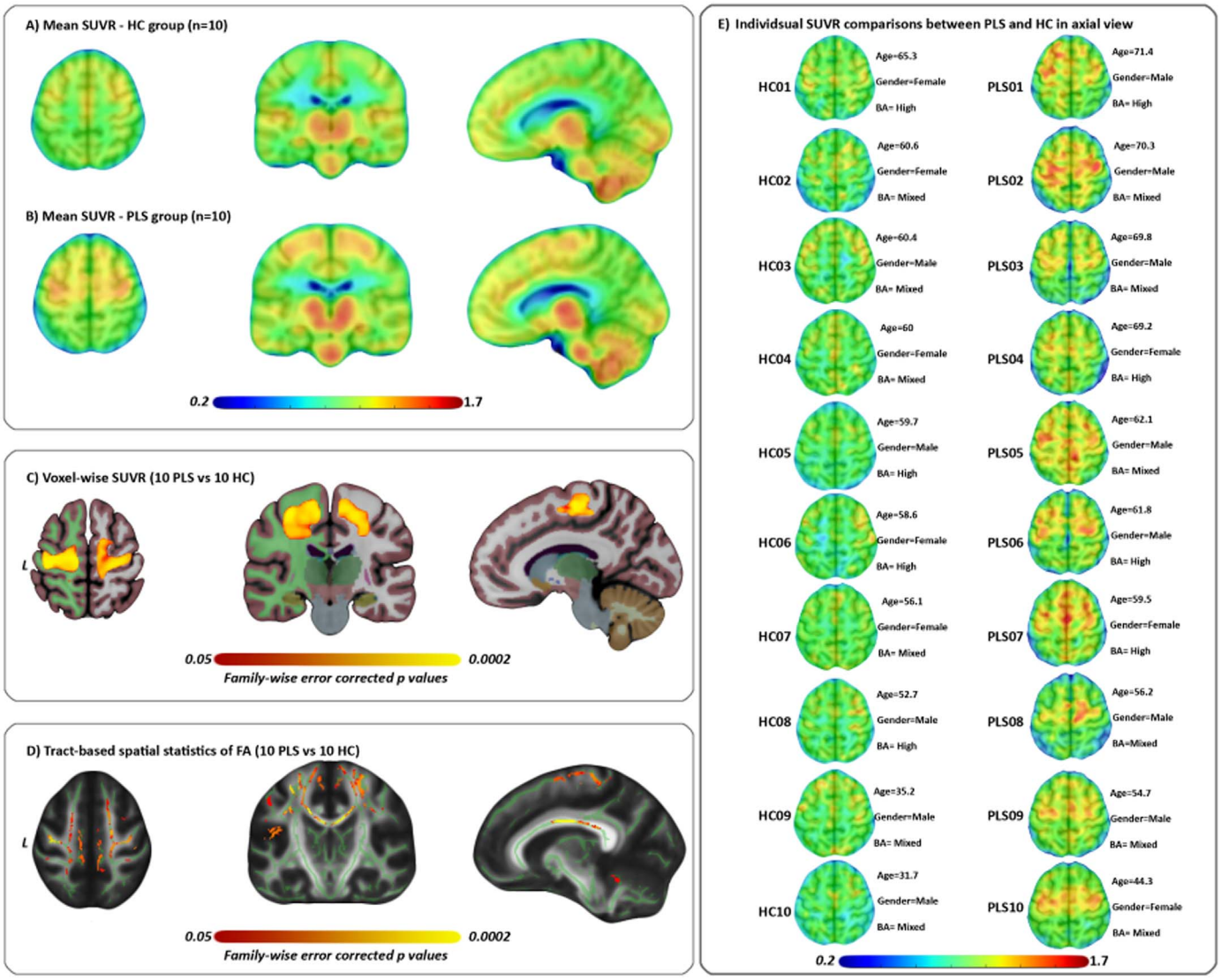

Fig. 1. [^{11}C]-PBR28 uptake images and statistical maps for between-group differences.
Panel A and B: Mean [^{11}C]-PBR28 uptake (expressed as $SUVR_{60–90\ min}$) in ten PLS individuals (A) and ten healthy controls (HC) (B). The color bar represents [^{11}C]-PBR28 uptake.
Panel C: Statistical maps comparing PLS and HC shows significantly higher [^{11}C]-PBR28 uptake in the motor regions in PLS compared to HC ($p_{FWE} < 0.05$). The color bar (red to yellow) represents higher [^{11}C]-PBR28 uptake in PLS as compared to HC.
All images are shown at MNI coordinates x = −10, y = −20, and z = +55.
Panel D: Tract-based spatial statistics analysis of FA maps shows decreased FA values in multiple white matter tracts in 10 PLS participants compared to 10 healthy controls. The color bar red-yellow represents decreased FA in PLS compared to controls. The mean FA white matter skeleton generated by TBBS for all participants in the study is shown in green. Data is shown using the standard template FMRIB58 at coordinates x = −10, y = −22, z = +55.
Panel E: [^{11}C]-PBR28 uptake (expressed as $SUVR_{60–90\ min}$) in ten healthy controls (HC) and ten individuals with PLS. (For interpretation of the references to color in this figure legend, the reader is referred to the web version of this article.)

presence of neuroinflammation in the brain, it remains debated whether neuroinflammation drives the initial pathogenesis (Boillee et al., 2006) or occurs as a consequence of neurodegeneration, or both, in motor neuron diseases in general and PLS in particular. [^{11}C]-PBR28 is a radiotracer that can be used to visualize and measure neuroinflammation. However, [^{11}C]-PBR28 is not specific for microglia or their phenotypes. Thus, development of PET radioligands that are specific for microglia phenotypes is an unmet need and would greatly enhance the impact of this type of studies on our understanding of disease pathophysiology.

This study has additional limitations including the relatively small sample size, though previously published PET studies in other neurodegenerative diseases have shown disease-related changes with comparable sample sizes (Kreisl et al., 2016; Kreisl et al., 2013; Zurcher et al., 2015; Alshikho et al., 2016; Turner et al., 2004; Corcia et al., 2012; Politis et al., 2011; Tai et al., 2007; Coughlin et al., 2015; Coughlin et al., 2017). Given the small sample size, our findings should be considered as preliminary and warrant replication in larger cohorts. In addition, information about how glia activation evolves over time and whether these changes might be predictive of future disease progression is not available. Lastly, a potential limitation of the study is the use of SUVR to represent [^{11}C]-PBR28 binding without performing arterial sampling for kinetic modeling. The approach used here has been used successfully in previous studies (Zurcher et al., 2015; Alshikho et al., 2016; Herranz et al., 2016; Loggia et al., 2015; Nair et al., 2016) and is strengthened by recent data showing good correlation between SUVR and DVR computed using radiometabolite-corrected arterial input function (Herranz et al., 2016).

The area of highest [^{11}C]-PBR28 uptake in PLS was located in the subcortical white matter underlying the motor cortex and was therefore

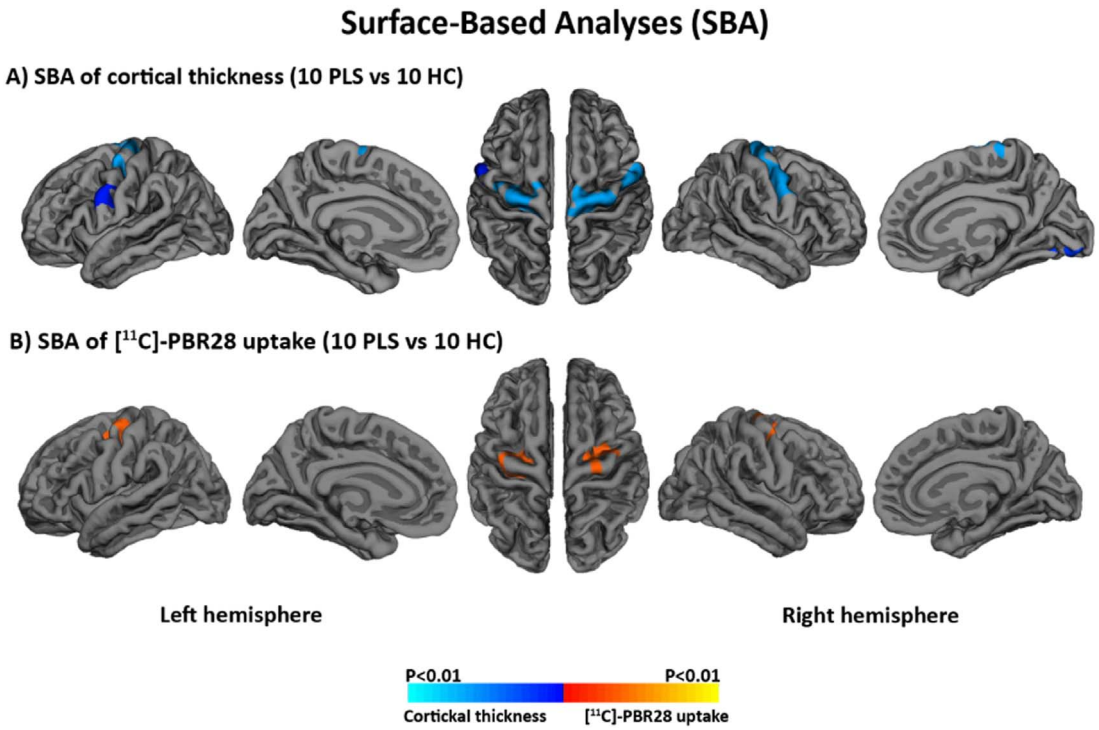

Fig. 2. Surface based analyses (SBA).
Panel A: SBA of cortical thickness shows cortical thinning in PLS compared to HC. The color bar (blue to cyan) represent the difference in cortical thickness between PLS and HC.
Panel B: SBA of [^{11}C]-PBR28 uptake shows increased [^{11}C]-PBR28 uptake in PLS compared to HC. The color bar (red to yellow) represent the difference in [^{11}C]-PBR28 uptake between PLS and HC.
Statistical maps were overlaid onto the pial surface of the left and the right hemispheres. The results of all SBA analyses were cluster-wise corrected for multiple comparisons ($p < 0.01$). (For interpretation of the references to color in this figure legend, the reader is referred to the web version of this article.)

partially outside the *a priori* ROI based on our previous ALS studies, where maximal [^{11}C]-PBR28 uptake was found in the cortex of the precentral and paracentral gyri (Zurcher et al., 2015; Alshikho et al., 2016). For this reason, the results of the ROI analyses may not describe the full extent of glia activation in PLS. Our study was instrumental in localizing the area of highest [^{11}C]-PBR28 uptake in PLS and will guide future projects to more accurately measure the extent of [^{11}C]-PBR28 uptake in PLS. [^{11}C]-PBR28 is a molecular marker of neuro-inflammation while FA is measure of white matter integrity and the two may serve different roles as PLS biomarkers. Thus, [^{11}C]-PBR28 may represent a dynamic measure of target engagement of compounds that affect neuroinflammatory pathways. Larger, longitudinal studies are urgently needed to establish whether [^{11}C]-PBR28 may be used as a pharmacodynamic biomarker in the context of PLS clinical trials.

Contrary to our results in ALS (Zurcher et al., 2015; Alshikho et al., 2016), we did not observe a correlation between [^{11}C]-PBR28 uptake and available clinical outcomes such as UMNB and the ALSFRS-R. The reasons for these findings are unclear and may relate to a ceiling effect of the UMNB when used to assess function in PLS. UMNB is measured by grading deep tendon reflexes and may have an insufficient dynamic range in PLS where reflexes are broadly elevated. The ALSFRS-R was developed and validated to measure function in ALS (Cedarbaum et al., 1999), where disability is driven not only by upper but also by lower motor neuron dysfunction. Preserved lower motor neuron function in PLS may underlie the lack of correlation between MR-PET measures and ALSFRS-R scores. Of note, no PLS-specific functional rating scale is available at the present time. Alternatively, these findings may reflect a different relationship between glia activation and neurodegeneration in PLS when compared to ALS. It should be noted that due to established PLS diagnostic criteria that require to wait a few years before diagnosing PLS (3 to 4 years depending on whether Pringle (Pringle et al., 1992) or Gordon (Gordon et al., 2006) criteria are used), our cohort comprised individuals whose mean disease duration was about 11 years, well beyond the 2-year disease duration of participants in our previous ALS study (Zurcher et al., 2015; Alshikho et al., 2016). Thus, the lack of an association between imaging metrics and clinical measures may be due to the late observation time, when clinical changes may no longer be associated with some of the mechanisms we investigated with imaging. Future studies are needed to determine the time course of [^{11}C]-PBR28 uptake early after onset of UMN-predominant disease.

In conclusion, we demonstrated that multimodal MR-PET can localize and quantify glia activation *in vivo* in patients with PLS. We propose that this approach may inform clinical drug development by providing a platform to screen candidate therapeutics that target glia activation. Large, multi-center, longitudinal studies are needed to validate MR-PET with [^{11}C]-PBR28 as a biomarker for PLS.

Study funded by a grant from the Spastic Paraplegia Foundation (PI: Paganoni), grants from the Harvard NeuroDiscovery Center (PI: Paganoni; PI: Atassi), grant 1K23NS083715-01A1 from NINDS (PI: Atassi) and the MGH PLS Fund.

Supplementary data to this article can be found online at https://doi.org/10.1016/j.nicl.2017.10.024.

Author contributions

Dr. Paganoni had full access to all the data in the study and takes responsibility for the integrity of the data and the accuracy of the data analysis.

Study concept and design: Dr. Paganoni, Dr. Zürcher, Dr. Loggia, Dr. Rosen, Dr. Cudkowicz, Dr. Hooker, Dr. Atassi.

Acquisition, analysis, or interpretation of data: All authors.

Drafting of the manuscript: Dr. Paganoni.

Critical revision of the manuscript for important intellectual content: All authors.

Statistical analysis: James Chan.

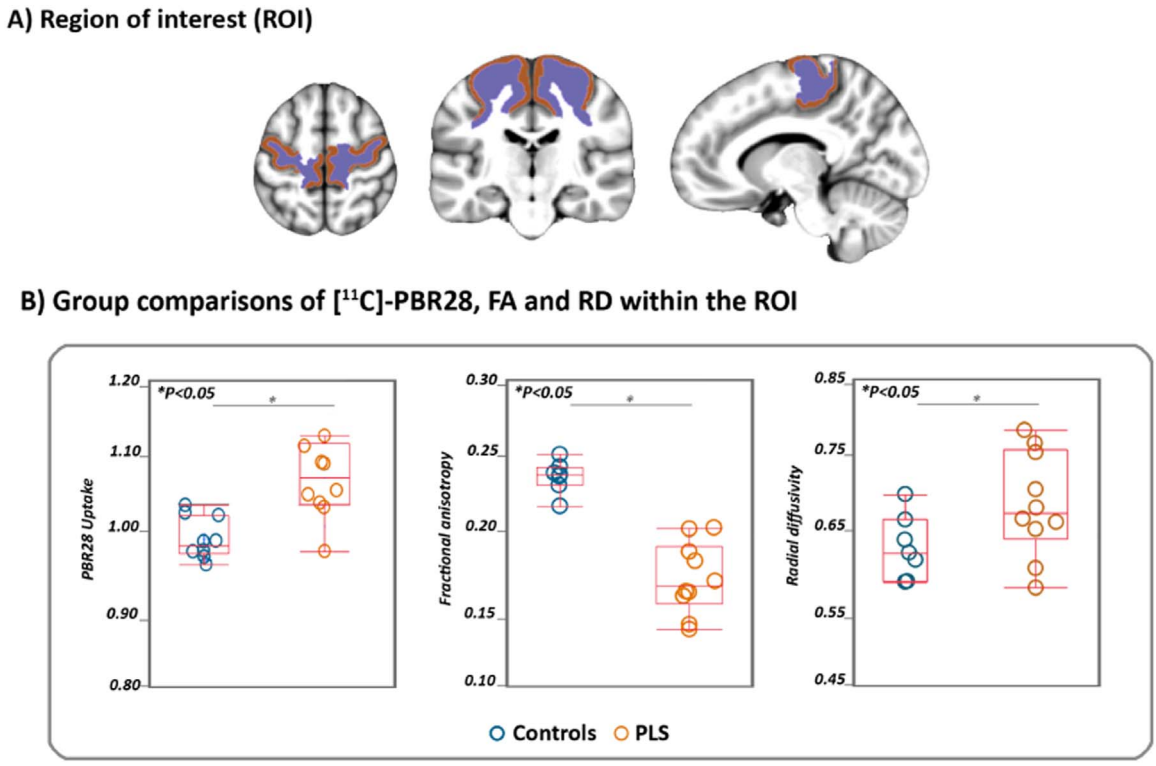

Fig. 3. Region of Interest (ROI) analyses.
Panel A: Representation of the ROI overlaid onto MNI152-1 mm standard space, and shown at MNI coordinates x = −10, y = −20, and z = +55. The ROI includes the bilateral precentral and paracentral gyri. Contribution from gray and subcortical white matter to the ROI is indicated in maroon and purple, respectively.
Panel B: Box plots showing [^{11}C]-PBR28 uptake, FA and RD values in PLS (orange circles) and HC (blue circles) within the ROI. The horizontal white line in each box plot represents the median (the box contains median, 25th, and 75th percentiles). The asterisk denotes significant group differences, at $p < 0.05$. The scale of RD values is divided by 1000. (For interpretation of the references to color in this figure legend, the reader is referred to the web version of this article.)

Obtained funding: Dr. Atassi, Dr. Paganoni.

Administrative, technical, or material support: Dr. Zürcher, Dr. Loggia.

Study supervision: Dr. Paganoni, Dr. Zürcher, Dr. Loggia, Dr. Rosen, Dr. Cudkowicz, Dr. Hooker, Dr. Atassi.

Acknowledgements

The authors wish to thank the A. A. Martinos Center for Biomedical Imaging Radiopharmacy and the NMR technicians Grae Arabasz, Shirley Hsu, and Regan Butterfield. We would also like to thank the Spastic Paraplegia Foundation for supporting innovation in PLS clinical care and research.

Author disclosures

Sabrina Paganoni has received research funding from Target ALS, the ALS association, ALS Finding a Cure, Amylyx, the Salah Foundation, The Harvard NeuroDiscovery Center, and the Spastic Paraplegia Foundation.

Mohamad J. Alshikho reports no disclosures.

Nicole R. Zürcher reports no disclosures.

Paul Michael Cernasov reports no disclosures.

Suma Babu reports no disclosures.

Marco L. Loggia reports no disclosures.

James Chan reports no disclosures.

Daniel B. Chonde reports no disclosures.

David Izquierdo-Garcia reports no disclosures.

Ciprian Catana reports no disclosures.

Caterina Mainero reports no disclosures.

Bruce R. Rosen reports no disclosures.

Merit E. Cudkowicz has provided consulting for Cytokinetics, Astra Zeneca, Lilly, Genentech, Biogen-IDEC, Voyager, and Biohaven.

Jacob M. Hooker reports no disclosures.

Nazem Atassi consulted for Biogen and Mitsubishi Tanabe.

Table 2
ROI analysis: between group comparisons of MR-PET measures.

Measures	HC	PLS	*p* value (Wilcoxon)	Cohen d (95% CI)
[^{11}C]-PBR28 $SUVR_{60–90\ min}$	0.97 (0.03)	1.07 (0.07)	0.0013[a]	1.86 (0.98 to 1.05)
FA	0.22 (0.04)	0.15 (0.03)	0.0097[a]	1.98 (0.16 to 0.20)
RD	0.55 (0.1)	0.67 (0.08)	0.035[a]	1.32 (0.56 to 0.68)
MD	0.62 (0.14)	0.72 (0.08)	0.18	0.87 (0.62 to 0.74)
AD	0.76 (0.18)	0.82 (0.09)	0.73	0.42 (0.73 to 0.86)

Values are presented as means (standard deviation).
Diffusivity values (RD, MD, AD) were adjusted to 0 decimals (multiplied by 1000).
Abbreviations: AD: axial diffusivity; CI: confidence interval; FA: fractional anisotropy; MD: mean diffusivity; RD: radial diffusivity; SUVR: standardized uptake value ratio.
[a] Significant difference between the groups.

References

Alexianu, M.E., Kozovska, M., Appel, S.H., 2001. Immune reactivity in a mouse model of familial ALS correlates with disease progression. Neurology 57 (7), 1282–1289.

Alshikho, M.J., Zurcher, N.R., Loggia, M.L., et al., 2016. Glial activation colocalizes with structural abnormalities in amyotrophic lateral sclerosis. Neurology 87 (24), 2554–2561.

Appel, S.H., Zhao, W., Beers, D.R., Henkel, J.S., 2011. The microglial-motoneuron dialogue in ALS. Acta Myol. 30 (1), 4–8.

Beal, M.F., Richardson Jr., E.P., 1981. Primary lateral sclerosis: a case report. Arch. Neurol. 38 (10), 630–633.

Beers, D.R., Henkel, J.S., Xiao, Q., et al., 2006. Wild-type microglia extend survival in PU.1 knockout mice with familial amyotrophic lateral sclerosis. Proc. Natl. Acad. Sci. U. S. A. 103 (43), 16021–16026.

Boillee, S., Yamanaka, K., Lobsiger, C.S., et al., 2006. Onset and progression in inherited ALS determined by motor neurons and microglia. Science 312 (5778), 1389–1392.

Brettschneider, J., Toledo, J.B., Van Deerlin, V.M., et al., 2012. Microglial activation correlates with disease progression and upper motor neuron clinical symptoms in amyotrophic lateral sclerosis. PLoS One 7 (6), e39216.

Brier, M.R., Gordon, B., Friedrichsen, K., et al., 2016. Tau and Abeta imaging, CSF measures, and cognition in Alzheimer's disease. Sci. Transl. Med. 8 (338), 338ra366.

Butman, J.A., Floeter, M.K., 2007. Decreased thickness of primary motor cortex in primary lateral sclerosis. AJNR Am. J. Neuroradiol. 28 (1), 87–91.

Canu, E., Agosta, F., Galantucci, S., et al., 2013. Extramotor damage is associated with cognition in primary lateral sclerosis patients. PLoS One 8 (12), e82017.

Cedarbaum, J.M., Stambler, N., Malta, E., et al., 1999. The ALSFRS-R: a revised ALS functional rating scale that incorporates assessments of respiratory function. BDNF ALS Study Group (Phase III). J. Neurol. Sci. 169 (1–2), 13–21.

Corcia, P., Tauber, C., Vercoullie, J., et al., 2012. Molecular imaging of microglial activation in amyotrophic lateral sclerosis. PLoS One 7 (12), e52941.

Coughlin, J.M., Wang, Y., Munro, C.A., et al., 2015. Neuroinflammation and brain atrophy in former NFL players: an in vivo multimodal imaging pilot study. Neurobiol. Dis. 74, 58–65.

Coughlin, J.M., Wang, Y., Minn, I., et al., 2017. Imaging of glial cell activation and white matter integrity in brains of active and recently retired National Football League Players. JAMA Neurol. 74 (1), 67–74.

Franciosi, S., Ryu, J.K., Shim, Y., et al., 2012. Age-dependent neurovascular abnormalities and altered microglial morphology in the YAC128 mouse model of Huntington disease. Neurobiol. Dis. 45 (1), 438–449.

Gomperts, S.N., Locascio, J.J., Makaretz, S.J., et al., 2016. Tau positron emission tomographic imaging in the Lewy body diseases. JAMA Neurol. 73 (11), 1334–1341.

Gordon, P.H., Cheng, B., Katz, I.B., et al., 2006. The natural history of primary lateral sclerosis. Neurology 66 (5), 647–653.

Griciuc, A., Serrano-Pozo, A., Parrado, A.R., et al., 2013. Alzheimer's disease risk gene CD33 inhibits microglial uptake of amyloid beta. Neuron 78 (4), 631–643.

Herranz, E., Gianni, C., Louapre, C., et al., 2016. Neuroinflammatory component of gray matter pathology in multiple sclerosis. Ann. Neurol. 80 (5), 776–790.

Hua, K., Zhang, J., Wakana, S., et al., 2008. Tract probability maps in stereotaxic spaces: analyses of white matter anatomy and tract-specific quantification. NeuroImage 39 (1), 336–347.

Hudson, A.J., Kiernan, J.A., Munoz, D.G., Pringle, C.E., Brown, W.F., Ebers, G.C., 1993. Clinicopathological features of primary lateral sclerosis are different from amyotrophic lateral sclerosis. Brain Res. Bull. 30 (3–4), 359–364.

Imaizumi, M., Kim, H.J., Zoghbi, S.S., et al., 2007. PET imaging with [11C]PBR28 can localize and quantify upregulated peripheral benzodiazepine receptors associated with cerebral ischemia in rat. Neurosci. Lett. 411 (3), 200–205.

Iwata, N.K., Kwan, J.Y., Danielian, L.E., et al., 2011. White matter alterations differ in primary lateral sclerosis and amyotrophic lateral sclerosis. Brain 134 (Pt 9), 2642–2655.

Kreisl, W.C., Lyoo, C.H., McGwier, M., et al., 2013. In vivo radioligand binding to translocator protein correlates with severity of Alzheimer's disease. Brain 136 (Pt 7), 2228–2238.

Kreisl, W.C., Lyoo, C.H., Liow, J.S., et al., 2016. (11)C-PBR28 binding to translocator protein increases with progression of Alzheimer's disease. Neurobiol. Aging 44, 53–61.

Kwan, J.Y., Meoded, A., Danielian, L.E., Wu, T., Floeter, M.K., 2012. Structural imaging differences and longitudinal changes in primary lateral sclerosis and amyotrophic lateral sclerosis. Neuroimage Clin. 2, 151–160.

Lavisse, S., Inoue, K., Jan, C., et al., 2015. [18F]DPA-714 PET imaging of translocator protein TSPO (18 kDa) in the normal and excitotoxically-lesioned nonhuman primate brain. Eur. J. Nucl. Med. Mol. Imaging 42 (3), 478–494.

Liao, B., Zhao, W., Beers, D.R., Henkel, J.S., Appel, S.H., 2012. Transformation from a neuroprotective to a neurotoxic microglial phenotype in a mouse model of ALS. Exp. Neurol. 237 (1), 147–152.

Loggia, M.L., Chonde, D.B., Akeju, O., et al., 2015. Evidence for brain glial activation in chronic pain patients. Brain 138 (Pt 3), 604–615.

Nair, A., Veronese, M., Xu, X., et al., 2016. Test-retest analysis of a non-invasive method of quantifying [(11)C]-PBR28 binding in Alzheimer's disease. EJNMMI Res. 6 (1), 72.

Owen, D.R., Yeo, A.J., Gunn, R.N., et al., 2012. An 18-kDa translocator protein (TSPO) polymorphism explains differences in binding affinity of the PET radioligand PBR28. J. Cereb. Blood Flow Metab. 32 (1), 1–5.

Passamonti, L., Vazquez Rodriguez, P., Hong, Y.T., et al., 2017. 18F-AV-1451 positron emission tomography in Alzheimer's disease and progressive supranuclear palsy. Brain 140 (3), 781–791.

Politis, M., Pavese, N., Tai, Y.F., et al., 2011. Microglial activation in regions related to cognitive function predicts disease onset in Huntington's disease: a multimodal imaging study. Hum. Brain Mapp. 32 (2), 258–270.

Pringle, C.E., Hudson, A.J., Munoz, D.G., Kiernan, J.A., Brown, W.F., Ebers, G.C., 1992. Primary lateral sclerosis. Clinical features, neuropathology and diagnostic criteria. Brain 115 (Pt 2), 495–520.

Ramlackhansingh, A.F., Brooks, D.J., Greenwood, R.J., et al., 2011. Inflammation after trauma: microglial activation and traumatic brain injury. Ann. Neurol. 70 (3), 374–383.

Rupprecht, R., Papadopoulos, V., Rammes, G., et al., 2010. Translocator protein (18 kDa) (TSPO) as a therapeutic target for neurological and psychiatric disorders. Nat. Rev. Drug Discov. 9 (12), 971–988.

Sapp, E., Kegel, K.B., Aronin, N., et al., 2001. Early and progressive accumulation of reactive microglia in the Huntington disease brain. J. Neuropathol. Exp. Neurol. 60 (2), 161–172.

Statland, J.M., Barohn, R.J., Dimachkie, M.M., Floeter, M.K., Mitsumoto, H., 2015. Primary lateral sclerosis. Neurol. Clin. 33 (4), 749–760.

Tai, Y.F., Pavese, N., Gerhard, A., et al., 2007. Microglial activation in presymptomatic Huntington's disease gene carriers. Brain 130 (Pt 7), 1759–1766.

Tartaglia, M.C., Laluz, V., Rowe, A., et al., 2009. Brain atrophy in primary lateral sclerosis. Neurology 72 (14), 1236–1241.

Turner, M.R., Cagnin, A., Turkheimer, F.E., et al., 2004. Evidence of widespread cerebral microglial activation in amyotrophic lateral sclerosis: an [11C](R)-PK11195 positron emission tomography study. Neurobiol. Dis. 15 (3), 601–609.

Vargas, M.R., Johnson, J.A., 2010. Astrogliosis in amyotrophic lateral sclerosis: role and therapeutic potential of astrocytes. Neurotherapeutics 7 (4), 471–481.

Wakana, S., Caprihan, A., Panzenboeck, M.M., et al., 2007. Reproducibility of quantitative tractography methods applied to cerebral white matter. NeuroImage 36 (3), 630–644.

Yin, Z., Raj, D., Saiepour, N., Van Dam, D., Brouwer, N., Holtman, I.R., Eggen, B.J.L., Möller, T., Tamm, J.A., Abdourahman, A., Hol, E.M., Kamphuis, W., Bayer, T.A., De Deyn, P.P., Boddeke, E., 2017. Immune hyperreactivity of Aβ plaque-associated microglia in Alzheimer's disease. Neurobiol. Aging 55, 115–122. http://dx.doi.org/10.1016/j.neurobiolaging.2017.03.021. (Epub 2017 Mar 27).

Zhao, W., Xie, W., Le, W., et al., 2004. Activated microglia initiate motor neuron injury by a nitric oxide and glutamate-mediated mechanism. J. Neuropathol. Exp. Neurol. 63 (9), 964–977.

Zurcher, N.R., Loggia, M.L., Lawson, R., et al., 2015. Increased in vivo glial activation in patients with amyotrophic lateral sclerosis: assessed with [(11)C]-PBR28. Neuroimage Clin. 7, 409–414.